Journal of Solid State Chemistry **145,** 587–603 (1999)
Article ID jssc.1999.8240, available online at http://www.idealibrary.com on IDEAL®

Spin Glass Magnetism in the Oxygen-Rich $La_2Co_xCu_{1-x}O_{4+\delta}$ Layered Oxides: Magnetic Susceptibility and Muon-Spin-Relaxation Studies

Alexandros Lappas,* Kosmas Prassides,*,[1] Fredy N. Gygax,† and Alexander Schenck†

*School of Chemistry, Physics and Environmental Science, University of Sussex, Brighton BN1 9QJ, UK; and Institute for Particle Physics, Swiss Federal Institute of Technology (ETH) Zurich, CH-5232 Villigen PSI, Switzerland

Received December 11, 1998; in revised form February 19, 1999; accepted February 25, 1999

A series of oxygen-rich phases with formal stoichiometry $La_2Co_xCu_{1-x}O_{4+\delta}$ has been prepared. The excess of oxygen defects ($0.06 \leq \delta \leq 0.20$) that can be accommodated in the structure is higher than that found in the parent superconducting $La_2CuO_{4+\delta}$ phase. The ac and dc susceptibility measurements reveal a rich magnetic phase diagram. The early members of the series ($x \leq 0.25$) order antiferromagnetically with localized magnetic moments per ion site of 0.5 μ_B. The ordering temperature T_N is rapidly reduced and the boundary of the paramagnetic-to-antiferromagnetic (AF) phase transition is smeared out as the cobalt content increases from $x = 0.25$ to 0.5. Further increase of the cobalt content ($0.5 \leq x \leq 0.90$) leads to suppression of the AF state and the appearance of a spin glass at very low temperatures. This is attributed to the increased degree of structural and electronic disorder among (Co/Cu) sites, which leads to frustration of the nearest-neighbor (*nn*) AF bonds. The spin glass phases of the $La_2Co_{0.5}Cu_{0.5}O_{4.18}$ ($T_f = 18$ K) and $La_2Co_{0.75}Cu_{0.25}O_{4.16}$ ($T_f = 30$ K) were also investigated by the muon spin relaxation (μ^+SR) technique. When T_f is approached from above, the μ^+ spin dynamics show a nonexponential relaxation described by a power-law dependence of the muon spin polarization, $G(t) = A_0 e^{-(\lambda_d t)^\beta}$. The observed rapid growth of the correlation times τ_c is reminiscent of the spin freezing process in Ising spin glasses. A continuous drop in the value of the exponent β is also encountered, changing from 1.0 (simple exponential) at $T \sim 3.3$ T_f to 0.5 (square root exponential) at $T \sim 1.3$ T_f, and finally approaching 1/3 very close to T_f. A variety of chemical systems that undergo a spin glass transition are governed by spin dynamics that follow a universal picture similar to the one encountered here.

1. INTRODUCTION

It is widely accepted that properties such as superconductivity and magnetism in the Cu–O based high-T_c materials are critically related to the oxygen vacancy concentration, which may be controlled by varying the synthetic conditions. The discovery of high-temperature superconductivity in $La_2CuO_{4+\delta}$ with $T_c \approx 38$ K further increased the interest in copper–oxygen chemistry. The question of how the excess oxygen in the crystal can transform a Mott–Hubbard insulator, such as stoichiometric La_2CuO_4, into a metal, undergoing a transition to a superconducting state, needed thorough investigation. Therefore, alternative ways to study the behavior of the excess oxygen in the lattice were sought by employing high-pressure methods, room temperature chemical oxidation (1), and electrochemical intercalation techniques (2), in addition to synthesizing a series of isostructural compounds, such as $La_2NiO_{4+\delta}$ (3), where a large amount of extra oxygen could easily be accommodated. In a similar way, a significant amount of excess lattice oxygen can be incorporated without phase separation into the isomorphous Co-containing compounds, because of the greater accessibility of oxidation states greater than 2+. In an effort to further probe the role of the oxygen nonstoichiometry in the mechanism of superconductivity, we have synthesized a series of compounds where Co ions substitute for Cu^{2+} in the Cu–O layers. The series of materials with nominal stoichiometry $La_2Co_xCu_{1-x}O_{4+\delta}$ ($0.05 \leq x \leq 1.0$) was prepared. A significant amount of excess oxygen ($\delta \leq 0.20$) was easily accommodated without the need for high-pressure oxygenation.

Even though layered perovskites of the $A_2BO_{4+\delta}$ type with the K_2NiF_4 structure have been extensively studied, there is still controversy concerning the nature of the incorporated excess lattice oxygen. For the nickelate series, it was proposed (4) that sufficient space exists in the lattice between AO layers for the excess oxygen to be incorporated as an interstitial peroxide unit, O_2^{2-} coordinated to four A^+ ions. Further studies attempted to characterize in detail the oxygen species in $La_2CuO_{4+\delta}$. Schirber *et al.* (5) identified the extra charged oxygen as superoxide ions, O_2^-, with X-ray photoelectron studies further supporting this observation (6). The latter technique also showed that the near-surface region was considerably enriched in these excess oxygen species. However, Zhou *et al.* (7) argued that their

[1] To whom correspondence should be addressed.

0022-4596/99 $30.00

identification was indeed associated with superficial oxygen and not with bulk interstitial O_2^- species. Subsequent neutron powder diffraction studies (8, 9) concluded that the excess oxygen is accommodated in superconducting $La_2CuO_{4+\delta}$ in the form of oxide ions, O_2^-, which are responsible for the doping mechanism. A significantly different model was proposed for lightly overdoped $La_{1.84}Sr_{0.16}CuO_{4+\delta}$ (10), with neutral oxygen O atoms accounting for the extra oxygen in the material, and thus not contributing to hole formation. Finally, oxygenated $La_{2-x}Sr_xCuO_{4+\delta}$ ($x < 0.15$) prepared by room temperature chemical oxidation (11) resulted in a much larger oxygen content ($0.05 < \delta < 0.14$) than that obtained by earlier high-pressure synthetic efforts. The authors suggested that two different oxygen species may be present in the chemically oxidized samples, oxide ions, and neutral O atoms. However, their materials show no phase separation.

In order to probe the role of excess oxygen in the electronic properties of layered copper-based oxides, we have synthesized the series $La_2Co_xCu_{1-x}O_{4+\delta}$ in which Co substitutes for Cu^{2+} in the Cu–O planes. A much higher oxygen solubility ($0.06 \leq \delta \leq 0.20$) than that found in $La_2CuO_{4+\delta}$ ($\delta < 0.05$) was achieved without the need for high-pressure oxygenation. TGA measurements confirmed the deviation from ideal stoichiometry ($\delta = 0$). We have already employed high resolution neutron powder diffraction to monitor the evolution of the crystal structure upon variation of both Co concentration and oxygen content in certain members of this series. The extra oxygen was found to form an interstitial defect in a similar fashion to the prototypical $La_2CuO_{4+\delta}$ system, but no phase separation takes place in these mixed Co/Cu-containing solids. The neutron data allowed us to investigate in detail the coordination of the oxygen defect, establishing that it is consistent with negatively charged O^{2-} ions (12).

Here we report on the complex magnetic behavior displayed by the randomly mixed $La_2Co_xCu_{1-x}O_{4+\delta}$ system. Macroscopic ac and dc susceptibility measurements reveal a very rich magnetic phase diagram with a crossover from a long range antiferromagnetic (AF) to a spin glass (SG) state. We find that strong nearest-neighbor (*nn*) magnetic superexchange interactions in the Cu-rich materials ($x \leq 0.25$) are responsible for the AF order of localized electronic moments ($\sim 0.5\ \mu_B$) in the $(Cu/Co)O_2$ planes, in a manner similar to that in the parent La_2CuO_4 phase. With increasing Co content ($x > 0.25$), the Néel state is rapidly suppressed because of an increased degree of disorder among the transition metal sites and frustration due to competition between antiferromagnetic and/or ferromagnetic interactions of *nn* ions. Eventually a site-random magnetic system is formed, and the 3D Néel state is replaced by a new magnetic state, characterized by short-range random order, reminiscent of a spin glass (for compositions $x = 0.5$–0.9). The microscopic physical mechanisms involved were further probed by means of zero-field (ZF) and longitudinal-field (LF) muon spin relaxation (μ^+SR) techniques for the $x = 0.50$ and 0.75 compositions. It was shown that characteristics of a system liable to undergo a transition to a spin-glass state were present: a nonexponential decay (i.e., stretched exponential) of the dynamic spin correlation function and a rapid growth of the correlation times on approaching the freezing temperature (T_f) from above. It is suggested that ferromagnetic clusters can be the building blocks out of which the SG state develops at very low temperatures. Our results add further insight to the spin-freezing process observed in diverse classes of chemical systems and reflect a more universal behavior encountered in a variety of other spin glasses. Finally, the important role of the strong magnetic frustration in layered transition metal oxides was demonstrated by the behavior of $La_2CoO_{4+\delta}$, which is isostructural (13) with $La_2CuO_{4+\delta}$. We find that AF order appears below $T_N \sim 75$ K, in contrast to the stoichiometric compound ($\delta \sim 0$), which orders at 275 K (14).

2. EXPERIMENTAL

a. Synthesis

Ceramic oxides with composition $La_2Co_xCu_{1-x}O_{4+\delta}$ were synthesized using the solution-based citrate sol-gel technique. The solution techniques have proven advantageous as they result in highly homogeneous dopant distributions, and therefore the oxide products are more uniformly mixed, than those prepared from oxide precursors. Samples (10 g) were prepared by mixing stoichiometric amounts of the powdered metal nitrates ($La(NO_3)_3 \cdot 6H_2O$, $Co(NO_3)_2 \cdot 3H_2O$, $Cu(NO_3)_2 \cdot 3H_2O$) with citric acid in distilled water—an appropriate amount of ethylene glycol was also added. The resulting gel was decomposed into a solid and thoroughly ground into a fine powder, which was pressed into pellets. The series of samples prepared had cobalt-to-copper ratios ranging from 0.05:0.95 to 1.0:0.0. In the initial stage of the heating procedure, all compositions were calcined in an alumina boat at 650°C in air for 24 hr. However, as the cobalt concentration was increased, it was found that these reaction conditions did not result in single phase materials. This was attributed to the easy oxidation of Co^{2+} to higher oxidation states. In order to prepare compounds with higher cobalt concentrations and effective oxidation states as close to $+2$ as possible, it was found necessary to exclude oxidizing media and perform the synthesis under slightly reducing conditions. The pelletized material was thus placed in a tube furnace at room temperature under a continuous CO_2 gas flow. The furnace was then switched on, gradually reaching the target temperature (within 1–2 hr). The annealing temperature and duration varied among the series, but the adopted synthetic procedure was the same. Finally, the specimen was left to cool

TABLE 1
Preparation Conditions for the $La_2Co_xCu_{1-x}O_{4+\delta}$ Siries

	Temperature/°C, annealing/h, atmosphere		
x	Stage #1	Stage #2	Stage #3
0.05	650, 24, air	950, 48, air	—
0.10	650, 24, air	950, 48, air	—
0.25	650, 24, air	950, 48, air	1200, 24, CO_2
0.50	650, 24, air	1200, 24, CO_2	1250, 24, air
0.75	650, 24, air	1150, 24, CO_2	—
0.90	650, 24, air	1200, 48, CO_2	1400, 24, CO_2
1.0	650, 24, air	1200, 48, CO_2	1400, 24, CO_2

down slowly (over a period of 6–8 hr) in the CO_2 atmosphere. CO_2 gas was kept flowing through the various stages of the heating procedure. Intermediate regrinds (every 24 hr of annealing) and firings were essential in improving homogeneity and achieving phase purity. Table 1 gives the details of the synthetic route followed for the $La_2Co_xCu_{1-x}O_{4+\delta}$ series.

b. Characterization

X-ray powder diffraction was used to monitor the progress of the reactions and confirm the monophasic character of the products. Diffraction patterns were collected with a Siemens D-5000 diffractometer with CuK_α radiation. To a first approximation, the diffraction patterns indexed well in terms of the parent K_2NiF_4 structure (space group $I4/mmm$), but with variations in the lattice constants. However, at very low ($x \sim 0.10$) and very high ($x \sim 0.90$) Co concentration, it appeared that an orthorhombic supercell of the tetragonal K_2NiF_4 structure was appropriate. Rietveld refinements of high-resolution neutron powder diffraction data (12, 13) helped to verify the correct crystallographic symmetry and orthorhombic distortion for all the compositions studied between 4.5 K and room temperature. However, with increasing Co content we find a crossover at $x = 0.50$ from the *Bmab* space group, which supports ordered tilts of the (Cu/Co)O_6 octahedra, to the *Fmmm* symmetry, which involves disordered tilts. Figure 1 shows the composition evolution of the basal plane lattice parameters a and b at very low temperatures, the inset shows the corresponding orthorhombic distortion, $[(b-a)/(b+a)]$ (13).

The overall oxygen content of the samples was determined by thermogravimetric reduction using a Perkin–Elmer TGA-7 instrument. As detailed in earlier work (12), X-ray powder diffraction was employed to determine the phases involved. The weight-loss curves for coblat concentrations greater than about $x = 0.5$ show a well-defined temperature plateau between 450 and 650°C, suggesting stabilization of the stoichiometric $La_2Co_xCu_{1-x}O_{3.99}$ composition (Fig. 2a). However, the plateau gradually narrows and eventually turns into an inflexion region between about 370 and 470°C. This points to the formation of an intermediate phase with a substantially reduced oxygen content and formal stoichiometry $La_2Co_xCu_{1-x}O_{3.69}$ for $x \leq 0.5$ (Fig. 2b). A compilation of the thermogravimetric analysis results are presented in Table 2. The oxygen content per formula unit is always greater than 4 and increases with increasing Co concentration, x, indicative of the easy oxidation of the cobalt ions.

Preliminary magnetic susceptibility measurements were performed with an ac susceptometer (Model 7000 LakeShore series) between 4.5 and 300 K, in a magnetic field of $H_{AC} = 1$ Oe and a frequency, $\nu = 111.1$ Hz at the Cryophysics Ltd. Laboratories, UK. A dc method employing a Quantum Design SQUID magnetometer (AT&T Bell Laboratories, USA) was also employed to measure the susceptibility of the polycrystalline powdered samples (~ 180 mg) down to liquid helium temperatures, following zero-field-cooled (ZFC) and field-cooled (FC) protocols in an external field $B_{DC} = 1$T.

The problem of the existence of nonzero internal local fields in the low-temperature phases of $La_2Co_xCu_{1-x}O_{4+\delta}$ was addressed by using spin-polarized positive muons (μ^+) in the absence of external fields. The μ^+SR experiments

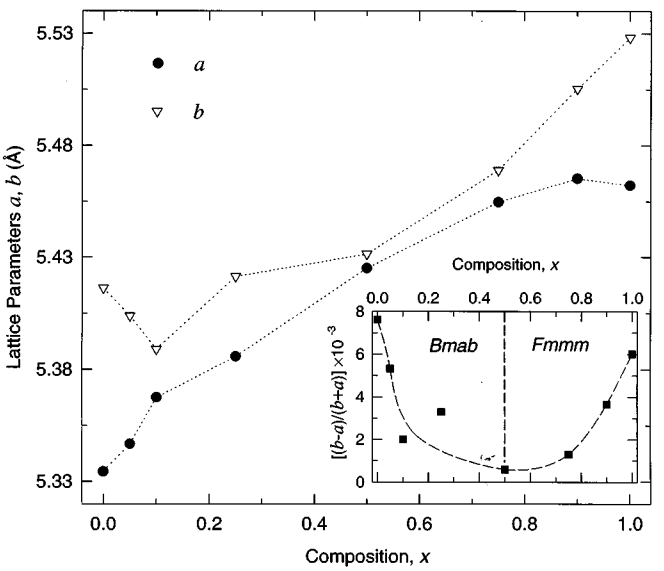

FIG. 1. Concentration dependence of the basal plane lattice parameters a and b of the orthorhombic unit cell in $La_2Co_xCu_{1-x}O_{4+\delta}$. *Inset*: The orthorhombic distortion $[(b-a)/(b+a)]$ as a function of Co content, x. The dashed vertical line at $x = 0.50$ signals the change in the symmetry of the orthorhombic cell from a B-centered (space group: *Bmab*, $x < 0.5$) to an F-centered lattice (spaces group: *Fmmm*, $x \geq 0.5$). The parameters are derived from Rietveld refinements of neutron diffraction data at 4.5 K, except for $x = 0.10$ and 0.25, which are at 45 and 50 K, respectively.

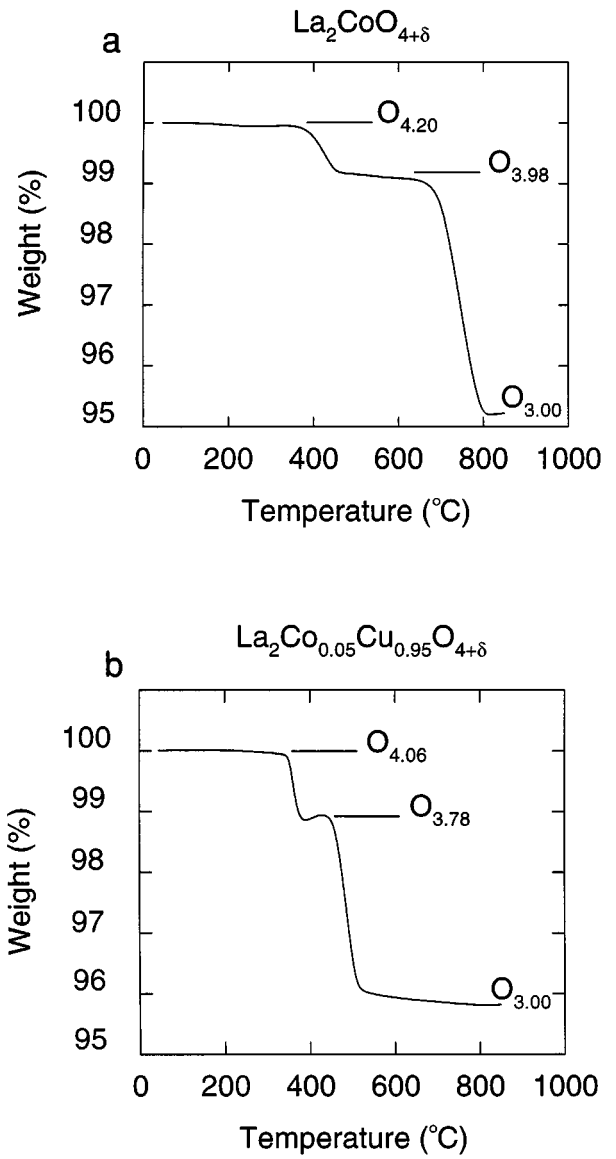

FIG. 2. Representative thermogravimetric weight-loss curves for the $La_2Co_xCu_{1-x}O_{4+\delta}$ samples ($x = 0.05$ and 1.0) heated in a flowing Ar–H_2 gas mixture.

were carried out at the Paul Scherrer Institute, Villigen, Switzerland, using a He-flow cryostat (GPS spectrometer) on the μ^+SR dedicated πM3 beamline of the PSI-600 MeV proton accelerator. The powdered samples were pressed into pellets and attached to the cryostat cold finger. The muons are implanted in the solid sample, and after they come to rest at an interstitial site, they act as highly sensitive microscopic local magnetic probes. In the presence of local magnetic fields, $\langle B_\mu \rangle$, they will precess with a frequency $\nu_\mu = (\gamma_\mu/2\pi)/\langle B_\mu \rangle$, where $(\gamma_\mu/2\pi) = 13.55$ kHz/G is the muon gyromagnetic ratio. In the absence of an applied external field, the appearance of a precession signals the onset of a magnetic ordering transition. Moreover, application of a magnetic field parallel to the initial muon spin polarization (longitudinal field) allows the decoupling of the μ^+-spin from the static internal field components. The μ^+SR technique in its various variants has proven extremely powerful in the field of small-moment magnetism, and in all cases when magnetic order is random, very short range, spatially inhomogeneous, or incommensurate (15).

3. RESULTS AND DISCUSSION

a. Magnetic Susceptibility Studies

The raw $\chi(T)$ data were first converted to molar susceptibility and then corrected for the core diamagnetic susceptibility of all elements in every compound. The temperature dependence of the inverse molar (dc) magnetic susceptibility for $La_2Co_{0.05}Cu_{0.95}O_{4.06}$ and $La_2Co_{0.10}Cu_{0.90}O_{4.14}$ is presented in Fig. 3, with the FC curve overlaying that of the ZFC data. The relatively short linear high temperature region, characteristic of Curie–Weiss behavior, $\chi = C/(T - \Theta)$, where Θ is the Weiss constant, gives rise to a pronounced "dip" that shifts toward lower temperatures with increasing cobalt concentration, i.e., it appears at $T \sim 220$ K for $x = 0.05$ and it broadens for $x = 0.10$ and shifts to $T \sim 190$ K. The slope obtained by a least-squares fit (Table 3) to the high-temperature Curie–Weiss part of the χ^{-1} vs T plot, corresponds to effective magnetic moments $\mu_{eff} = 0.41\ \mu_B$ for $x = 0.05$ and $\mu_{eff} = 0.51\ \mu_B$ for $x = 0.10$; these are much reduced from the magnitude of the spin-only value of 1.73 μ_B expected for an $S = 1/2$ system. The origin of the reduced value of the magnetic moment is the strong mixing (covalency) of the Cu $3d_{x^2-y^2}$ with the $2p_x$, $2p_y$ orbitals of the surrounding oxygen ions. The extra oxygen in the lattice may frustrate the superexchange interactions by the introduction of holes in the Co/Cu–O layers, which could lead to smaller localized moments.

The plots for both materials are reminiscent of the χ^{-1} vs T plot of La_2CuO_4. Such a behavior may be associated with transition of the Cu moments to an AF ordered

TABLE 2
Oxygen Content in the $La_2Co_xCu_{1-x}O_{4+\delta}$ series, as Determined by Thermogravimetric Analysis

x	Weight (mg)	Weight loss (%)	$\delta/\pm 0.02$
0.05	55.881	4.190	0.06
0.10	52.197	4.494	0.14
0.25	55.223	4.338	0.10
0.50	52.380	4.678	0.18
0.75	53.680	4.599	0.16
0.90	56.544	4.801	0.21
1.0	53.775	4.795	0.20

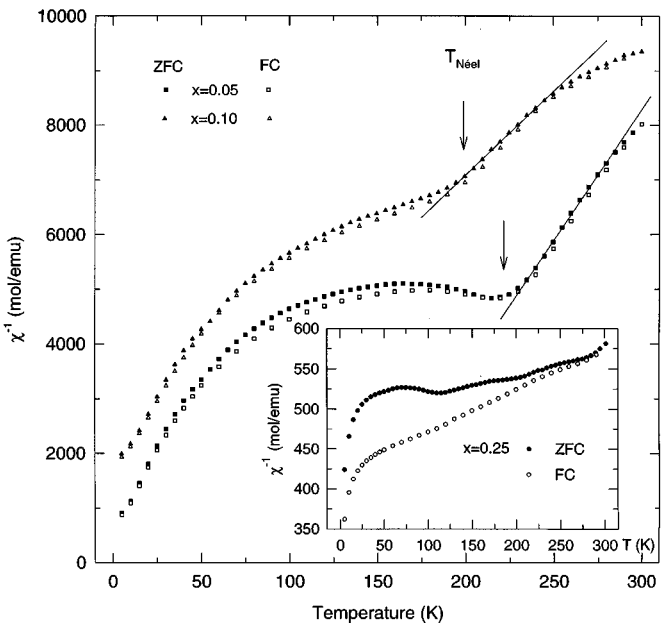

FIG. 3. The temperature dependence of the inverse molar (dc) magnetic susceptibility, χ^{-1} for $La_2Co_{0.05}Cu_{0.95}O_{4.06}$ and $La_2Co_{0.10}Cu_{0.90}O_{4.14}$. The latter is offset by 1000 for clarity. The "anomaly" related to the transition to the antiferromagnetically ordered state is indicated. The solid straight lines are the best fit curves characteristic of a Curie–Weiss behavior. *Inset*: temperature dependence of the field-cooled (FC) and zero-field cooled (ZFC) inverse magnetic susceptibility χ^{-1} of $La_2Co_{0.25}Cu_{0.75}O_{4.10}$.

state, similar to the one in the parent La_2CuO_4 phase ($T_N \sim 300$ K, with the Néel state being very sensitive to the oxygen content). Another feature in the present data is the sharp increase in the susceptibility below ~ 100 K, which was also observed in polycrystalline La_2CuO_4 samples. It could be attributed to a Curie–Weiss contribution (with a molar Curie constant of 0.0165(5) emu K/mol for $x = 0.05$ and 0.0176(3) emu K/mol for $x = 0.10$) of approximately 4.4 and 4.7% of near-isolated Co^{2+}/Cu^{2+} paramagnetic "impurities" with $S = 1/2$ in $La_2Co_{0.05}Cu_{0.95}O_{4.06}$ and $La_2Co_{0.10}Cu_{0.90}O_{4.14}$, respectively.

The inverse molar (DC) magnetic susceptibility of $La_2Co_{0.25}Cu_{0.75}O_{4.10}$ differs substantially from that in the earlier samples (Fig. 3 inset). Zero field cooled (ZFC) and field cooled (FC) data show significant hysteresis. The ZFC susceptibility, in contrast to the FC one, is nonlinear, showing deviation from the simple Curie–Weiss law; thus, we were unable to extract a reliable effective magnetic moment. The substantial hysteretic behavior between ZFC and FC data indicates that the magnetic state may be dominated by randomly frozen moments. The ZFC "anomaly" at ~ 100 K indicates that the order is short-range, with the antiferromagnetic transition heavily suppressed compared to earlier members ($x = 0.05$, 0.10) of the $La_2Co_xCu_{1-x}O_{4+\delta}$ family.

With a further increase in the cobalt concentration, such an effect disappears from the temperature dependence of the susceptibility, and a Curie–Weiss behavior is obeyed down to low temperatures. The ZFC curve has a minimum at ~ 9 K for $x = 0.50$, which shifts toward higher temperatures with decreasing Cu content, i.e., to ~ 30 K for $x = 0.75$ and ~ 18 K for $x = 0.90$ (Fig. 4, inset). Figure 4 presents the temperature dependence of the inverse molar (DC) magnetic susceptibility of $La_2Co_{0.50}Cu_{0.50}O_{4.18}$, $La_2Co_{0.75}Cu_{0.25}O_{4.16}$, and $La_2Co_{0.90}Cu_{0.10}O_{4.21}$. These curves differ from those in the lightly Co-"doped" materials, and it is interesting to note the substantially increased susceptibility for these compounds. The gradient of the χ^{-1} curve decreases a little at higher temperatures, giving rise to different linear regions. From a least-squares fit of the data of the $x = 0.50$ sample between 55 and 200 K, the molar Curie constant was estimated as 0.62 emu K/mol, whereas for $215 < T < 300$ K it was found to increase to 0.83 emu K/mol. Then the effective magnetic moment per Co/Cu cation was calculated as 2.23 and 2.58 μ_B for the respective temperature regions. Increasing Co content resulted in even larger values of the effective moment. An average value of 3.15 μ_B was found for the $x = 0.75$ composition, whereas for $x = 0.90$, it decreases from a value of 3.66 μ_B between $210 < T < 300$ K to 3.41 μ_B in the range extending down to 40 K. The best fit of the Curie–Weiss law at these temperatures resulted in negative values for the Weiss constant, Θ, which may well indicate short-range AF interactions in the paramagnetic phase of the compounds. These values together with the Curie constants and μ_{eff} are listed in Table 3.

TABLE 3
Magnetic Susceptibility Parameters Obtained from Fits to a Curie–Weiss Law[a]

x	Weight (mg)	Fitting interval (K)	C (emu K/mol)	Θ (K)	μ_{eff} (μ_B)	SSR
0.05	174	235–285	0.0209(2)	127.1(1.6)	0.409(2)	1.137
0.10	173	200–250	0.0324(4)	3.2(2.8)	0.509()	0.757
0.50*	600	33–94	0.436(5)	− 20.6(9)	1.87(1)	1.043
0.50	183	55–200	0.624(3)	− 34.2(7)	2.234(5)	0.619
		215–300	0.831(7)	− 111.9(3.1)	2.58(1)	0.213
0.75	165	110–200	1.203(7)	− 0.9(8)	3.102(9)	0.200
		215–300	1.276(6)	− 16.8(1.4)	3.195(8)	0.119
0.90	188	40–210	1.457(2)	− 53.9(2)	3.413(2)	0.064
		210–300	1.678(19)	− 95.4(3.9)	3.66(2)	0.121
1.0	186	80–110	2.16(13)	− 450(33)	4.16(3)	0.056
		130–220	9.72(24)	− 2424(64)	8.82(11)	0.040

[a] The weight of the sample used in the measurements, the temperature interval over which the least-sqaures fit was determined, the Curie constant C, the Weiss constant Θ, the effective magnetic moment μ_{eff} per Co/Cu cation, and the sum of squares of the residuals *SSR* giving an indication of the quality of fit are shown. (*) reports the fit results for the ac susceptibility of the 50% Co-containing sample.

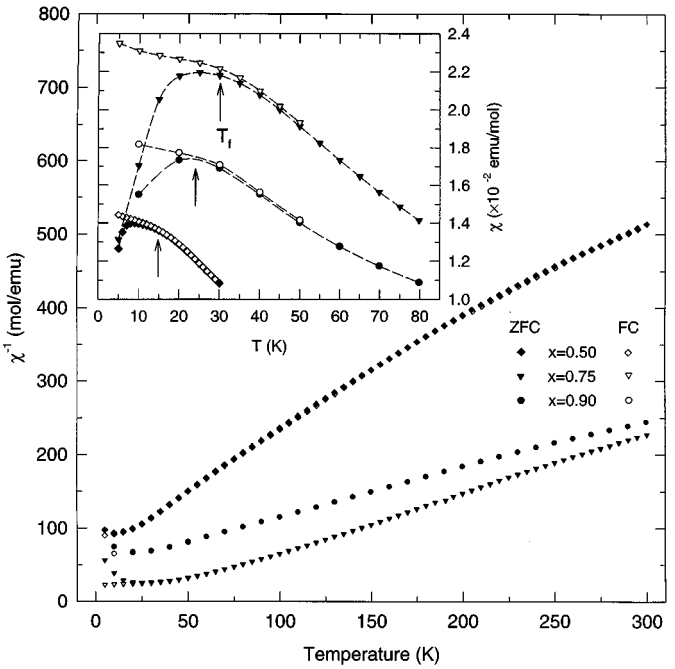

FIG. 4. The temperature dependence of the inverse molar (dc) magnetic susceptibility, χ^{-1} of the $La_2Co_xCu_{1-x}O_{4+\delta}$ samples ($x = 0.50, 0.75, 0.90$) as a function of temperature. The curves have been offset for clarity by $+20$, -20, $+10$ for $x = 0.50, 0.75, 0.90$, respectively. *Inset*: Temperature dependence of the molar (dc) magnetic susceptibility at $T \leq 80$ K for the $La_2Co_xCu_{1-x}O_{4+\delta}$ samples ($x = 0.50, 0.75, 0.90$). The divergence between the ZFC and FC data at low temperatures marks the onset of spin glass freezing in these materials.

The inverse molar (dc) magnetic susceptibility of the $La_2CoO_{4.20}$ compound versus temperature is plotted in Fig. 5. Deviation from linearity indicates a behavior different from that of a simple Curie–Weiss law; the shallow "dip" at ~ 70 K and the large negative Weiss constant(s), Θ, (>450 K, see Table 3) indicate the presence of AF correlations in this sample. Nonetheless, this temperature is substantially lower than the ordering temperature of 275 K found in the oxygen-stoichiometric phase (14). As with the lightly Co-"doped" members ($x = 0.05, 0.10$), a significant increase of the $La_2CoO_{4.20}$ susceptibility is observed at low temperatures. An attempt to calculate an effective magnetic moment from small linear χ^{-1} temperature ranges resulted in a large variation of its magnitude, i.e., $\mu_{eff} = 4.16\,\mu_B$ between 80 and 110 K, increasing to $8.82\,\mu_B$ when $130 < T < 220$ K.

b. Susceptibility and the Electronic Configurations of Co

Interpretation of the present magnetic data for the randomly mixed Co/Cu systems is complicated because of the plethora of electronic configurations available for the Co ions. The calculated values of μ_{eff} (Table 3) are clearly larger than the spin-only value of $1.73\,\mu_B$ for an $S = 1/2$ system. In order to understand the actual spin configuration of the Co ions, the effective magnetic moment per (Co/Cu) cation is recalculated (Table 4) under the assumption that it is mainly the oxidation state of Co that is affected by the excess oxygen, while Cu remains in a formal $2+$ valence state. If we assume that the extra oxygen is accommodated as discrete O^{2-} ions, as shown by high-resolution powder neutron diffraction (12), we can make use of the excess oxygen content, δ, as evaluated from the TGA measurements, to estimate the proportion of the Co^{2+} ions oxidized to Co^{3+} for $x = 0.50, 0.75, 0.90$, and 1.0 (Table 4). Variations in the oxidation and spin states of the cobalt ions and short-range spin clustering can account for deviations of the moments from those calculated according to the chemical composition.

The "wealth" of spin states for the transition metal ions and/or short-range clustering of spins may be responsible for the formation of a spin-glass-like phase that appears as a magnetic irreversibility (hysteresis) in the low-temperature part of the ZFC and FC susceptibilities of the $La_2Co_xCu_{1-x}O_{4+\delta}$ phases with $x = 0.50$, 0.75, and 0.90 (Fig. 4). The observed maximum in the ZFC data defines the freezing temperature, T_f. This effect can be in part rationalized in terms of the increased degree of disorder at the octahedral Co/Cu sites. Existence of frustration due to competition between antiferromagnetic and ferromagnetic superexchange interactions in this series also contributes to the appearance of the spin-glass state. These are characteristic properties of a randomly mixed ferromagnet (e.g.,

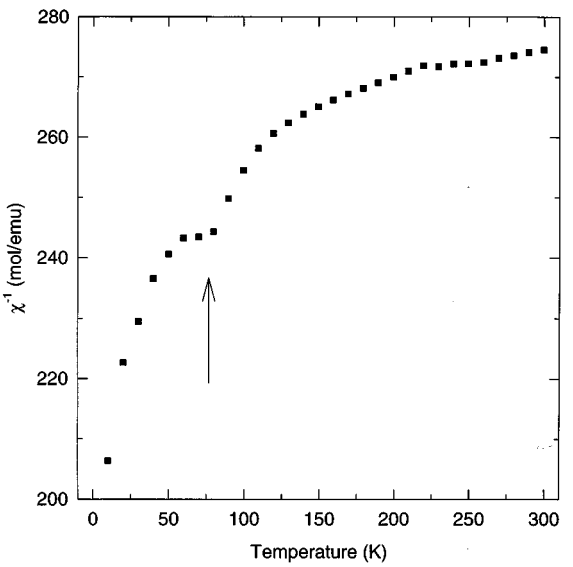

FIG. 5. The temperature dependence of the inverse molar (dc) magnetic susceptibility χ^{-1} for $La_2CoO_{4.20}$. The anomaly in susceptibility at ~ 70 K is related to an antiferromagnetic transition of the Co moments.

TABLE 4
"Ideal" Values for Spin-Only Effective Moment (μ_{eff}) per (Co/Cu) Cation Determined from Nominal Stoichiometries of the Co-Rich Members of the $La_2Co_xCu_{1-x}O_{4+\delta}$ family[a]

Nominal composition	$\mu_{eff}(\mu_B)$*	$\langle\mu_{eff}\rangle(\mu_B)$*	x	Fitting interval (K)	$\mu'_{eff}(\mu_B)$
$La_2(Co^{3+}_{0.4}Co^{2+}_{0.6})O_{4.20}$	4.28(35)	3.64(31)	1.0	80–110	4.16(13)
$La_2(Co^{3+}_{0.4}Co^{II}_{0.6})O_{4.20}$	3.00(27)				
$La_2(Co^{III}_{0.4}Co^{2+}_{0.6})O_{4.20}$	2.32(15)				
$La_2(Co^{3+}_{0.47}Co^{2+}_{0.53})_{0.90}Cu_{0.10}O_{4.21}$	4.09(35)	3.58(31)	0.90	40–210	3.413(2)
$La_2(Co^{3+}_{0.47}Co^{II}_{0.53})_{0.90}Cu_{0.10}O_{4.21}$	3.07(26)			210–300	3.66(2)
$La_2(Co^{III}_{0.47}Co^{2+}_{0.53})_{0.90}Cu_{0.10}O_{4.21}$	2.02(15)				
$La_2(Co^{3+}_{0.43}Co^{2+}_{0.57})_{0.75}Cu_{0.25}O_{4.16}$	3.67(35)	3.21(31)	0.75	110–200	3.102(9)
$La_2(Co^{3+}_{0.43}Co^{2+}_{0.57})_{0.75}Cu_{0.25}O_{4.16}$	2.75(26)			215–300	3.195(8)
$La_2(Co^{3+}_{0.43}Co^{II}_{0.57})_{0.75}Cu_{0.25}O_{4.16}$	2.09(15)				
$La_2(Co^{III}_{0.72}Co^{2+}_{0.28})_{0.50}Cu_{0.50}O_{4.18}$	3.17(35)	3.02(31)	0.50	55–200	2.234(5)
$La_2(Co^{3+}_{0.72}Co^{II}_{0.28})_{0.50}Cu_{0.50}O_{4.18}$	2.87(27)			215–300	2.58(1)
$La_2(Co^{III}_{0.72}Co^{2+}_{0.28})_{0.50}Cu_{0.50}O_{4.18}$	1.41(15)				

[a](*) The standard error in the calculated μ_{eff} arises from the experimental error in the oxygen content. The oxygen content found from TGA measurements is used to determine the oxidation state of cobalt, whereas formal valences are assumed for the other elements, La^{3+}, Cu^{2+}, and O^{2-}. According to Goodenough's convention, *arabic* and *latin* numbers indicate high- and low-spin states of Co ions, respectively. $\langle\mu_{eff}\rangle$ gives the average magnetic moment assuming coexistence of Co^{2+} and Co^{II} in these materials. μ'_{eff} is the effective magnetic moment found from least-squares fit of the susceptibility to a Curie–Weiss law (Table 3).

Rb_2CuF_4 (16)) with an isostructural antiferromagnet (e.g., Rb_2CoF_4 (17)) and predominant nearest-neighbor coupling, when they form a solid solution, as in $Rb_2Co_xCu_{1-x}F_4$ (18). Figure 6 compares the temperature variation of the ac and dc molar magnetic susceptibilities for the $La_2Co_{0.50}Cu_{0.50}O_{4.18}$ composition. The onset of spin freezing is clearly marked by a pronounced cusp at low temperatures.

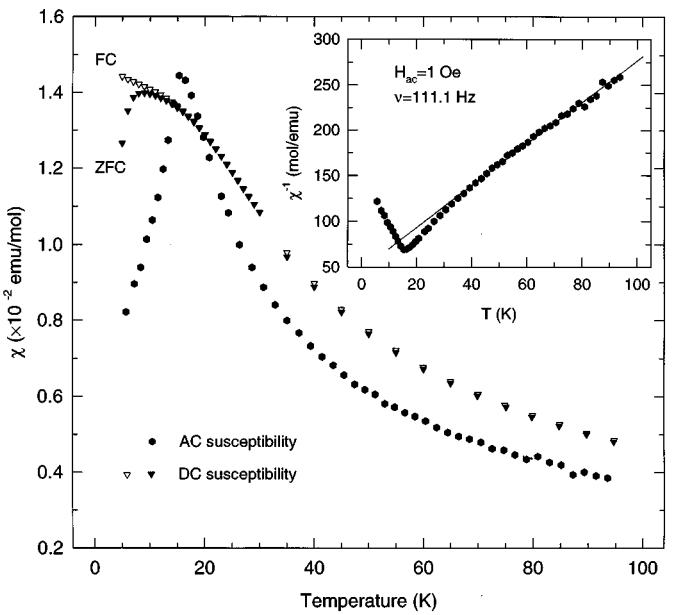

FIG. 6. The in-phase component (χ') of the ac magnetic susceptibility of $La_2Co_{0.50}Cu_{0.50}O_{4.18}$ vs temperature at 1 Oe and 111.1 Hz "driving" signal ($H_{DC} = 0$ Oe). The dc susceptibility (ZFC and FC conditions) of the same sample is overplotted. Both techniques determine the onset of the spin-glass freezing below about 18 K. *Inset*: Best fit of $1/\chi'$ curve to a Curie–Weiss law at high temperatures.

c. Muon Spin Relaxation Studies

Zero (ZF) and longitudinal field (LF) muon spin relaxation (μ^+SR) experiments were performed on the $La_2Co_xCu_{1-x}O_{4+\delta}$ phases with $x = 0.50$ and 0.75. These had shown hysteretic behavior between ZFC and FC susceptibility experiments at low temperatures (Fig. 4). μ^+SR data were collected using low-energy (surface) muons between 2.3 and 150 K. Positron intensities were recorded with a set of two counters in the forward (F) and backward (B) directions relative to the initial μ^+-spin polarization and the sample position. As the dc and ac data strongly suggest that the behavior of the samples is reminiscent of randomly mixed ferromagnetic–antiferromagnetic systems with predominantly nearest-neighbor coupling, we considered spin-glass models as candidates to explain the observed relaxation of the μ^+-spin polarization.

We start by giving a brief account of alternative relaxation functions that proved inadequate to describe the behavior of the μSR data. The divergence of ZFC and FC susceptibility data signaled the presence of a frozen-spin state below about 33 K for $La_2Co_{0.75}Cu_{0.25}O_{4.16}$. Accordingly, differing dynamic magnetic behavior would be expected to dominate the relaxation of the muon spin at

different temperatures, in a similar fashion to macroscopic magnetic measurements in analogous systems (19). Least-squares refinements of the ZF μ^+SR data for $La_2Co_{0.75}Cu_{0.25}O_{4.16}$ were initiated by employing a simple exponential function, $G(t) \sim A_0 \exp(-\lambda t)$ (L), appropriate for relatively fast fluctuating internal fields (15), to describe the time evolution of μ^+-spin polarization, $G(t)$ at $T \geq T_f$. Below T_f, $G(t)$ was described by a "root-exponential" function $G(t) \sim A_0 \exp(-\sqrt{\lambda t})$ appropriate for dilute spin glasses (20). In both cases, λ is the depolarization rate of the μ^+ spin. Such behavior had been observed in early μ^+SR studies of oxide spin glasses, such as $Fe_{2-x}Ti_{1+x}O_5$ (21). However, the root-exponential function proved inadequate to describe the data well at $T < T_f$. At the same time, a Gaussian function $G(t) \sim A_0 e^{-(\sigma^2 t^2)/2}$ (G) became more appropriate at elevated temperatures ($T \geq 80$ K), implying depolarization of the μ^+ spin by static randomly oriented nuclear dipolar fields. Such difficulties in modeling the data by a single functional form are expected if the μ^+ spin relaxation arises from spatially inhomogeneous depolarization mechanisms (22). For instance, this can occur when the presence of static random fields below the "glass" transition temperature, T_f, is replaced by rapidly fluctuating spin domains above T_f. These domains gradually grow, leading to paramagnetic behavior. Thus, we proceeded to explore two-component models for the description of the μ^+SR spectra (i.e., G + G at $T \leq 33$ K and G + L at $T > 33$ K). Careful inspection of the spectra below 20 K revealed that the very fast initial decay of the asymmetry recovered to a value equal to approximately one-third of its value at $t = 0$. However, there was still a shallow dip at about $t \sim 0.1$ μs, which could not be accounted for by either the G + G or the G + L combination.

So, we continued the data analysis of the ZF-μ^+SR spectra of $La_2Co_{0.75}Cu_{0.25}O_{4.16}$ by recalling that the observed behavior at low temperatures ($T < 20$ K) displays characteristic features of Kubo–Toyabe functions (23), for either Gaussian or Lorentzian distributions of static randomly oriented internal fields. The purely static Kubo–Toyabe function was not a good candidate because the 1/3-tail of the total asymmetry was decaying. Attempts to model this slow modulation of the random fields by a dynamic Kubo–Toyabe function (24, 25) also failed. Following the failure of all these models, we considered a more complicated lineshape arising from coexisting static and dynamic random local fields (26). A similar type of behavior, involving characteristics of Kubo–Toyabe-like relaxation has been reported earlier in several metallic spin-glass systems, like *Au*Fe (1.0 atomic%), and *Cu*Mn (1.1 and 5 atomic%) (27).

Based on the pioneering work of Edwards and Anderson (28) on spin glass behavior, Uemura *et al.* (29, 30) calculated an analytic expression for the ZF relaxation function of the μ^+ spin polarization in coexisting static and dynamic random fields:

$$G(t) = \frac{1}{3}\exp\left[-(4\alpha_d^2 t/\nu)^{1/2}\right] + \frac{2}{3}\left[1 - \frac{\alpha_s^2 t^2}{(4\alpha_d^2 t/\nu + \alpha_s^2 t^2)^{1/2}}\right]\exp\left[-(4\alpha_d^2 t/\nu + \alpha_s^2 t^2)^{1/2}\right]. \quad [1]$$

Equation [1] describes the depolarization of μ^+ in static random fields with spread α_s and coexisting rapidly fluctuating fields with a spread α_d. Assuming a full amplitude, $\alpha_0 = (\alpha_s^2 + \alpha_d^2)^{1/2}$, the Edwards–Anderson order parameter Q is given by

$$Q = \alpha_s^2/(\alpha_s^2 + \alpha_d^2). \quad [2]$$

Hence, in the limit of $\alpha_s \to 0$ and $Q \to 0$, Eq. [1] exhibits a "root-exponential" behavior, typical of rapid spin fluctuations with dynamic depolarization rate $\lambda_d = 4\alpha_d^2/\nu$ and ν the fluctuation rate of the magnetic moments. On the other hand, when $\alpha_d \to 0$ and $Q \to 1$, the depolarization of the μ^+ spin shows the characteristic lineshape of static random fields for a dilute spin system, $G(t) = \frac{1}{3} + \frac{2}{3}(1 - \alpha t)\exp(-\alpha t)$, where α/γ_μ is the half width at half maximum of the Lorentzian field distribution.

We therefore attempted to fit the ZF-μ^+SR time histograms of $La_2Co_{0.75}Cu_{0.25}O_{4.16}$ at $T < 33$ K with Eq. [1] using as variables the width α_s of the static random fields and the dynamic depolarization rate λ_d. The total zero-time asymmetry was determined at higher temperatures ($T > 50$ K) by fitting the spectra to a power-law function, $G(t) = A_0 e^{-(Dt)^\beta}$. The exponent β was left free to vary, resulting in very good fit quality (normalized $\chi^2 = 1.02$) and an accurate zero-time asymmetry. The forward and backward zero-time asymmetries were thus constrained during the fitting procedure to the high temperature values, $A_F = 20\%$ and $A_B = 19\%$, respectively. With this particular model, we obtained stable least-squares refinements and good agreement factors (on average, $\chi^2 = 1.02$). Figure 7 presents typical ZF-μ^+SR spectra and the corresponding best-fit curves at short times ($t < 1.0$ μs), confirming the validity of the model with coexisting static and dynamic random local fields below the "glass" transition temperature, T_f. The time evolution of the ZF muon spin polarization at 2.3 K for long times is shown as an inset in Fig. 7a and displays the characteristic slow decay of the 1/3-"tail" due to fluctuating field components below T_f.

A first indication of a drastic change in the lineshape of the μ^+ spin relaxation in $La_2Co_{0.75}Cu_{0.25}O_{4.16}$ was evident close to $T \sim 30$ K, since Eq. [1] failed to fit the spectra in this temperature regime. This was attributed to the

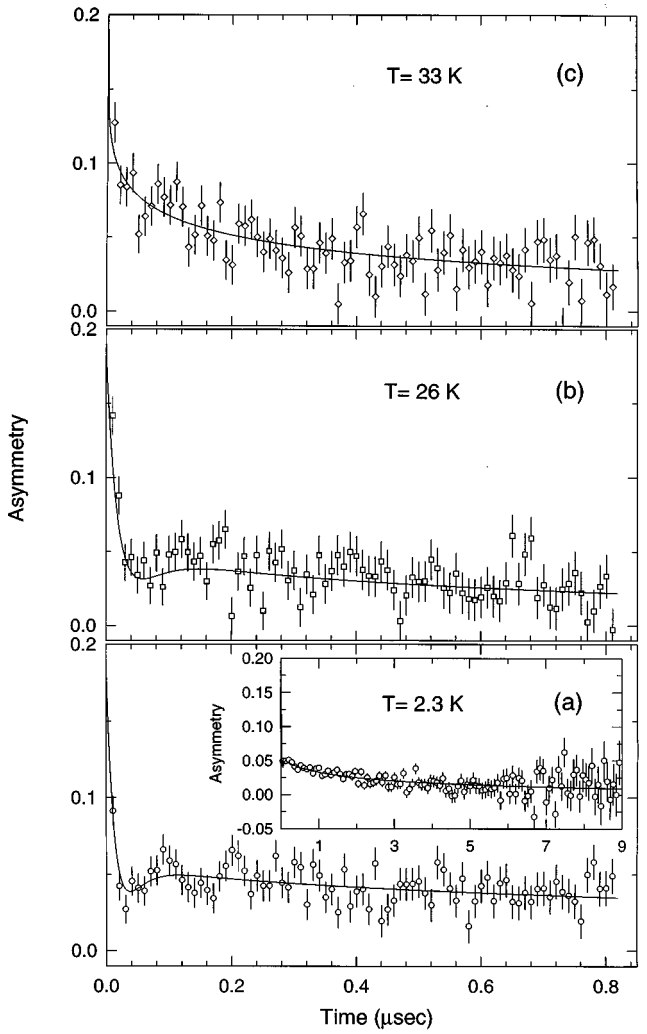

FIG. 7. Time evolution of the ZF μ^+-spin polarization for $La_2Co_{0.75}Cu_{0.25}O_{4.16}$ at various temperatures. The early parts of the time-dependent spectra are displayed. The solid lines represent the fits to the data with Eq. [1] ($2.3 \leq T < 33$ K) and Eq. [3] at $T \geq 33$ K, respectively. *Inset*: ZF-μ^+SR time-dependent asymmetry curve extending to long times.

transition to the temperature regime of rapid spin fluctuations, as expected from Eq. [1] in the limit of $Q \to 0$ with rising temperature. Assuming that the static random fields are gradually replaced by dynamic random fields when approaching some characteristic 'freezing transition' from below, Fig. 8 presents the temperature evolution of their field spread, α_s. The result is in agreement with the equation $\alpha_0 = (\alpha_s^2 + \alpha_d^2)^{1/2} = \alpha_s(T \to 0)$, which predicts that the static width is expected to reduce very quickly in magnitude as T approaches T_f from below (31).

Following the results of earlier simulations of Ogielski (32) for the dynamic (spin) correlation functions and their response in Ising spin-glass systems above T_f, we employed a "stretched exponential decay" of the form

$$G(t) = A_0 e^{-(\lambda_d t)^\beta} \qquad [3]$$

in subsequent least-squares refinements of the ZF-μSR spectra of $La_2Co_{0.75}Cu_{0.25}O_{4.16}$ at $T \geq 33$ K. This kind of power law appears to be a common feature of the glasslike behavior. It is familiar from relaxation in "ordinary" glasses, since it has been observed in several experimentally measured properties of spin-glass systems, for instance in the decay of the remnant magnetization (33), in the analysis of the dynamic susceptibility (34), in light scatterings studies of the dynamics in polymer solutions (35), and in the μ^+ spin depolarization in *Ag*Mn (7 atomic %) (36). The resulting fits are of excellent quality (Fig. 9), with χ^2 varying between 1.02 and 1.03. The zero-time asymmetry was kept constant as before.

The temperature evolution of the exponent β is given in Fig. 10a. It changes from $\frac{1}{3}$ very close to T_f to $\beta \sim 0.5$ (square-root exponential) just above 33 K, through $\beta \sim 1.0$ (simple exponential) to $\beta \sim 2.0$ (Gaussian-like) at temperatures around 150 K. Such behavior is reminiscent of the earlier work of Campbell *et al.* (36, 37) on the metallic spin-glass *Ag*Mn (7 atomic %) where the exponent was found to change from $\beta \sim 0.3$ at $T \sim T_f$ to $\beta \sim 1.0$ at room temperature. Recent μ^+SR work on the concentrated spin-glass $Y(Mn_{1-x}Al_x)_2$ (38) and the related alloys, β-$Mn_{1-x}Al_x$ (39) also revealed a similar behavior. These experimental findings for $\beta(T)$ are in close agreement with theoretical calculations (32, 40) of the power law behavior of

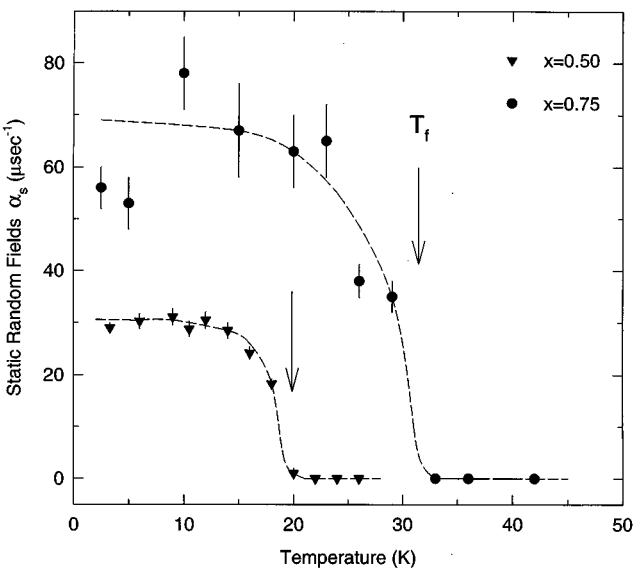

FIG. 8. Temperature dependence of the static width α_s of the internal field distribution at the muon site in $La_2Co_xCu_{1-x}O_{4+\delta}$ ($x = 0.50, 0.75$) spin glasses. α_s is zero above the freezing temperature T_f. The line through the data points is a guide to the eye.

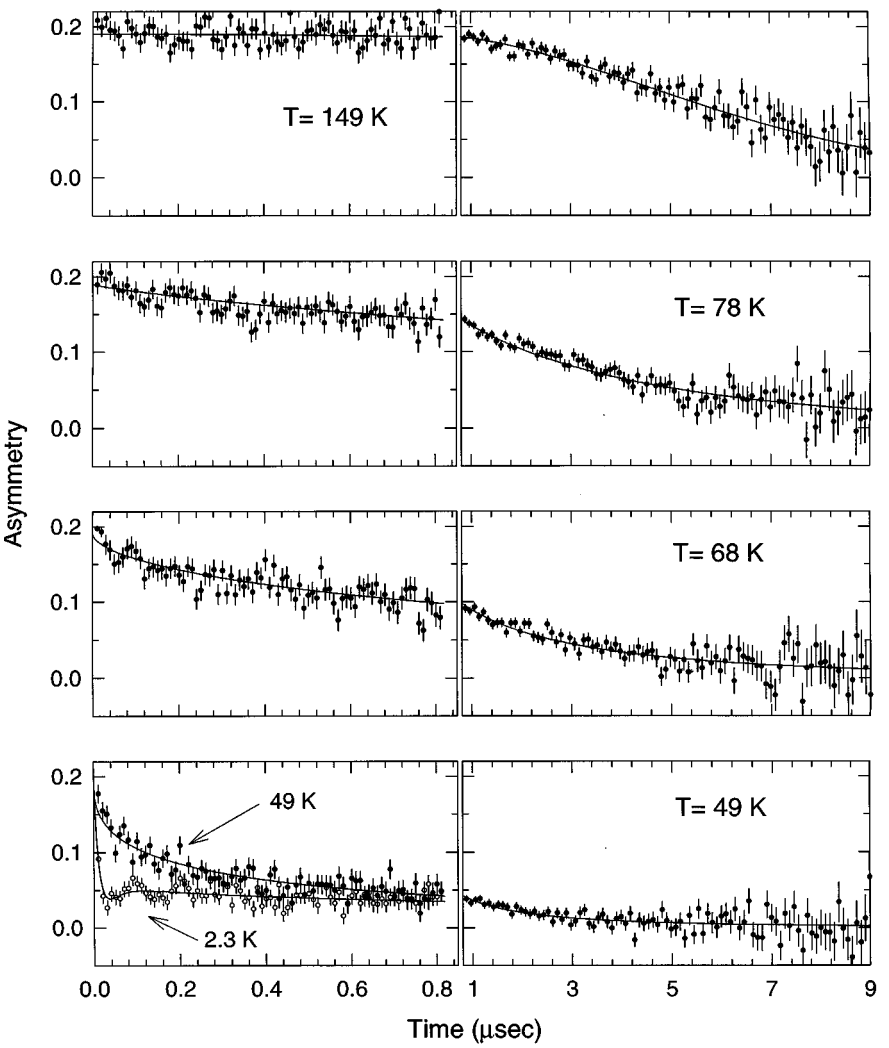

FIG. 9. Time evolution of the ZF μ^+-spin polarization for $La_2Co_{0.75}Cu_{0.25}O_{4.16}$ at temperatures above $T_f \sim 30$ K. The solid curve is a fit to the data with Eq. [3] ($T = 49$, 68, 78, and 149 K) and Eq. [1] ($T = 2.3$ K).

the (spin) correlation function in Ising spin-glasses. In the case of $La_2Co_{0.75}Cu_{0.25}O_{4.16}$, the deviation of $\beta(T)$ from unity at $T > 90$ K is attributed to nuclear dipole magnetic fields arising from Cu nuclei. The relaxation rate observed, $\sigma = 0.146(6)\ \mu s^{-1}$ at 150 K, is typical of the values found in most cuprates (41). Contribution from these fields becomes an increasingly important channel of μ^+ spin depolarization at elevated temperatures. Similar observations were reported by Uemura *et al.* (30) in the metallic spin glass *Cu*Mn at $T \sim 3T_f$.

Figure 11a presents the temperature dependence of the dynamic depolarization rate λ_d, as determined above and below 33 K, using Eq. [1] for coexisting static and dynamic random fields and the power law (Eq. [3]), respectively. The dynamic depolarization rate, λ_d, increases abruptly when T_f is approached from above, implying a rapid slowing down of the fluctuating random moments. The characteristic λ-shape clearly defines the "freezing transition" temperature, $T_f = 30$ K.

LF-μ^+SR measurements at an external field of 5 kOe were also undertaken for $La_2Co_{0.75}Cu_{0.25}O_{4.16}$ between 20 and 100 K. Such a large longitudinal field leads to decoupling of the muon spin from static random internal field components. The LF-μSR data were thus analyzed by employing a "power law" function (Fig. 12a). The exponent, β is close to $\sim 1/2$ (Fig. 10a) at temperatures approaching 30 K. The temperature dependence of the LF relaxation rate for $La_2Co_{0.75}Cu_{0.25}O_{4.16}$ is included in Fig. 11a, demonstrating the suppression of the static random field distribution.

μSR studies were also performed on another member of the present series, $La_2Co_{0.5}Cu_{0.5}O_{4.18}$. The temperature variation of the μ^+ spin depolarization in both ZF and LF 5 kOe) experiments shows pronounced features close to

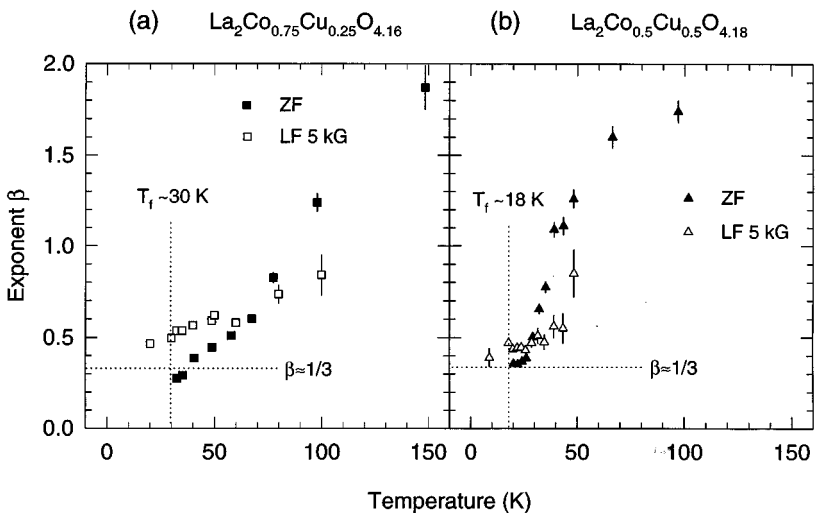

FIG. 10. Temperature evolution of the exponent β of the stretched exponential (Eq. [3]) form of the muon-spin relaxation above the freezing temperature T_f in the $La_2Co_xCu_{1-x}O_{4+\delta}$ ($x = 0.50, 0.75$) spin glasses.

the freezing temperature, $T_f \sim 18$ K. The ZF-μSR spectra were analyzed in a manner similar to that for $La_2Co_{0.75}Cu_{0.25}O_{4.16}$. The behavior (Fig. 13) is again consistent with that of an Ising spin glass, where a stretched exponential relaxation sets in below an upper characteristic temperature, T_f. As T approaches T_f, a continuous drop of β occurs, approaching $\sim \frac{1}{3}$ (Fig. 10b), whence an enhanced slowing down of the fluctuating magnetic moments is reflected in the divergence of the dynamic depolarization rate λ_d (Fig. 11b). At $T < T_f$, static random local fields coexist with dynamic ones. Uemura's function for spin glasses (Eq. [1]) was again used to model (Fig. 14) this particular field distribution. The temperature dependence of the static width, α_s, of the internal field distribution in $La_2Co_{0.5}Cu_{0.5}O_{4.18}$ is presented in Fig. 8. Finally, the results of the analysis of the LF-μ^+SR (at 5 kOe) spectra (Fig. 12b) between 9 and 70 K using the power-law function are included in Figs. 10b and 11b).

d. μ^+SR and Spin-Glass Dynamics above T_f

It is the distinct character of the evolution of the spin dynamics and relaxation above the freezing temperature that presents additional evidence for spin-glass behavior in

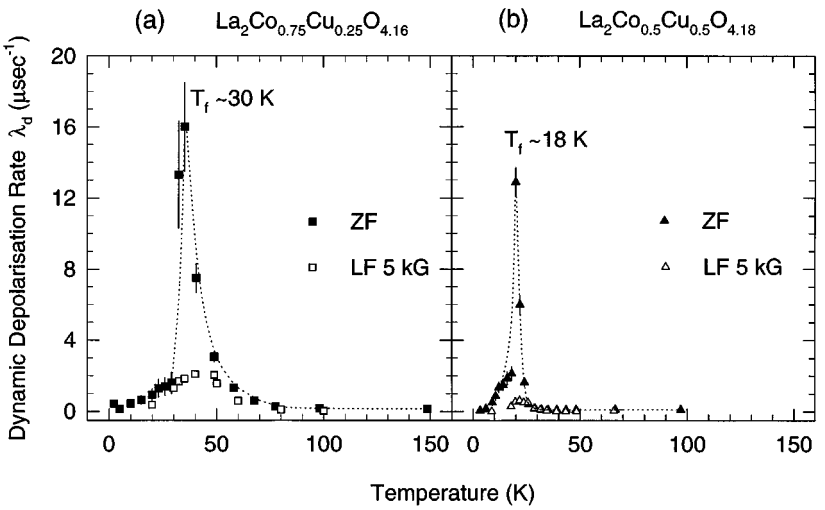

FIG. 11. The temperature dependence of the dynamic μ^+ spin depolarization rate λ_d in (a) $La_2Co_{0.75}Cu_{0.25}O_{4.16}$ and (b) $La_2Co_{0.50}Cu_{0.50}O_{4.18}$. Results for both zero-field (ZF = closed symbols) and longitudinal field (LF = open symbols) at 5 kOe are included.

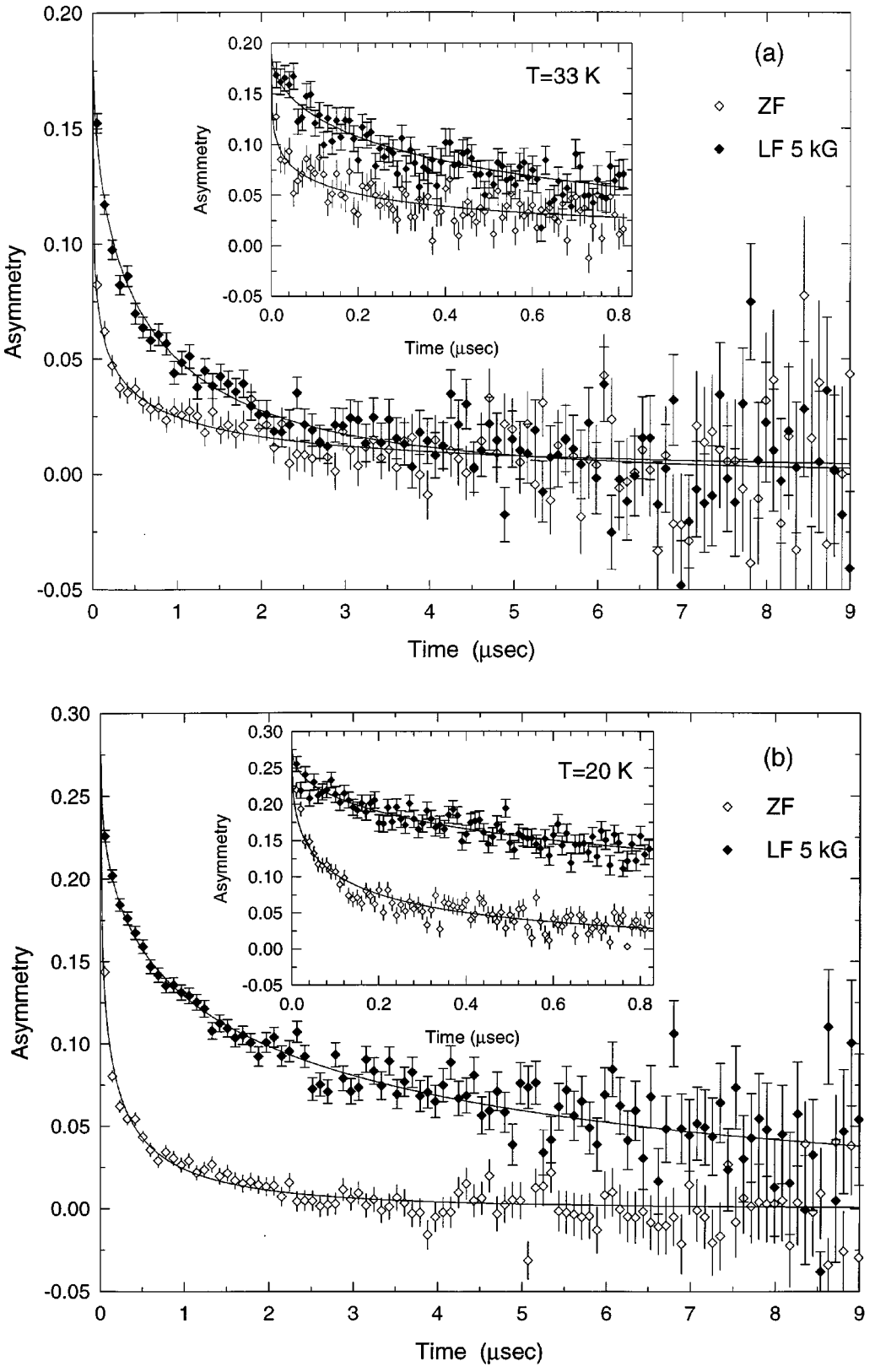

FIG. 12. Evolution of the μ^+ spin polarization for (a) $La_2Co_{0.75}Cu_{0.25}O_{4.16}$ at 33 K and (b) $La_2Co_{0.50}Cu_{0.50}O_{4.18}$ at 20 K in zero (ZF) and longitudinal (LF) field of 5 kOe. The solid lines represent the fits to the data with a power law function. The inset shows clearly that the LF partially decouples the muon spin depolarization from static field components.

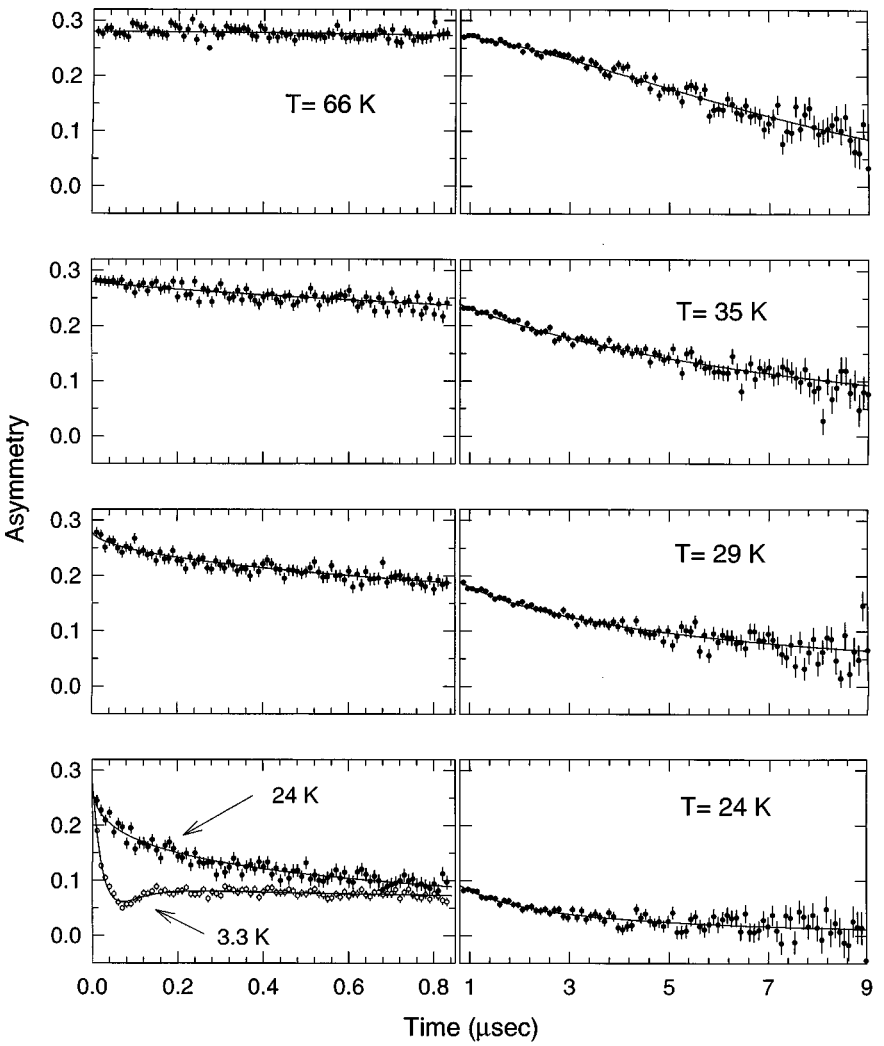

FIG. 13. Time evolution of the ZF μ^+-spin polarization for $La_2Co_{0.50}Cu_{0.50}O_{4.18}$ at temperatures above $T_f \sim 18$ K. The solid curves are fits to the data with Eq. [3] ($T = 24$, 29, 35, and 66 K) and Eq. [1] ($T = 3.3$ K).

the $La_2Co_xCu_{1-x}O_{4+\delta}$ ($x = 0.50$, 0.75) materials. Nonexponential decay of dynamic correlation functions and rapid growth of correlation times as the temperature approaches T_f from above have been clearly established. The T dependence of correlation times will be discussed in the following paragraphs. The nonexponential relaxation observed in these systems ($x = 0.50$, 0.75) is a direct consequence of the effect of disorder (40). The "stretched exponential" function (Eq. [3]) provides an excellent fit to numerous experiments in diverse glassy systems (42). For instance, mechanical relaxation in ordinary glasses and polymers can be analyzed in terms of stretched exponential relaxation with $\beta \sim 1/2$ to 1/3 near T_f (43).

Spin glasses can be thought of in terms of a large cluster, initially compact at high temperatures, that evolves with decreasing temperature to a ramified, noncompact, but percolating structure below some upper characteristic temperature. Finally, a fragmented and locally noncompact structure forms below T_f (40, 44). Numerical calculations for random-walk diffusion for the percolating cluster predict relaxation with a single characteristic time and exponential decay at high T. When the structure becomes ramified ($T \to T_f$), there are many characteristic lengths present and therefore a range of time scales (implying distribution of relaxation times), so relaxation takes place with a nonexponential form. It is found that for an Ising spin glass, stretched exponential relaxation sets in below an upper characteristic temperature above which $\beta \sim 1.0$. This is followed by a continuous drop in the value of β that tends to 1/3 as T is lowered toward T_f, where the correlation time diverges (45). Recent and earlier results (19) point to the universal character of the relaxation behavior for spin glasses, including the insulating $La_2Co_{0.5}Cu_{0.5}O_{4.18}$ and $La_2Co_{0.75}Cu_{0.25}O_{4.16}$ oxides.

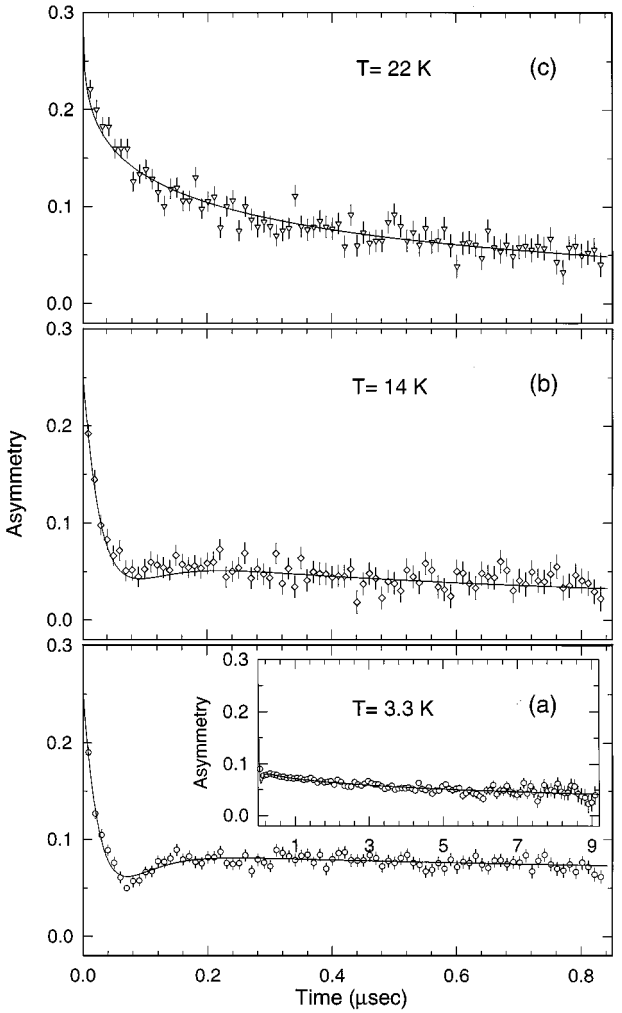

FIG. 14. Time evolution of the ZF μ^+-spin polarization for $La_2Co_{0.50}Cu_{0.50}O_{4.18}$ at various temperatures. The early parts of the time-dependent spectra are displayed. The solid lines represent the fits to the data with Eq. [1] ($3.3 \leq T < 20$ K) and Eq. [3] at $T \geq 20$ K, respectively. *Inset* in (a): ZF-μ^+SR time-dependent asymmetry curve extending to long times.

Information on the spin dynamics in $La_2Co_{0.5}Cu_{0.5}O_{4.18}$ and $La_2Co_{0.75}Cu_{0.25}O_{4.16}$ can be obtained by the temperature evolution of the dynamic depolarization rate, λ_d. Above T_f, where the random fields have no static component, $\alpha_s = 0$ (Fig. 8) the spread α_d of the rapidly fluctuating local fields becomes equal to the full amplitude, α_0. As the temperature is lowered below T_f, α_s grows toward a maximum value of α_0, at the expense of the dynamic field spread α_d. A rough estimate of α_0 can be taken from the average value of experimentally obtained α_s (Fig. 8) well below T_f, where the dynamic random fields have minimum contribution to the total field spread. For example, for the $x = 0.75$ composition, we find $\langle \alpha_0 \rangle \approx 64(6)\,\mu s^{-1}$, in good agreement with the calculated second moment of the local field distribution, $\sigma \approx 73\,\mu s^{-1}$. The latter was estimated by computing the dipolar fields acting on the μ^+ from local, randomly oriented Co^{2+} ($S = 3/2$) moments. The muon site was taken to be on the face of the orthorhombic unit cell of $La_2Co_{0.75}Cu_{0.25}O_{4.16}$, located ~ 1 Å away from the apical oxygen ions (46).

The average correlation time $\tau_c = 1/\nu$ of the fluctuating magnetic moments was calculated between 36 and 150 K for $x = 0.75$ (and 20 and 35 K for $x = 0.50$) with the expression $\lambda_d = 4\alpha_d^2/\nu$. The results are plotted in Fig. 15 against the reduced temperature, $(T - T_f)/T$. The correlation times for $La_2Co_{0.75}Cu_{0.25}O_{4.16}$ increase with decreasing temperature from $\tau_c = 7.8(5) \times 10^{-12}$ s ($\tau_c = 2.9(2) \times 10^{-11}$ s for $x = 0.50$) at $T \sim 3.3\,T_f$, toward $\tau_c = 7.5(1.2) \times 10^{-1}$ ($\tau_c = 1.7(1) \times 10^{-9}$ s for $x = 0.50$) at $T \sim 1.2\,T_f$. For spin glasses, there are several phenomenological and theoretical approaches (47) which attempt to describe the behavior of correlation time near the freezing temperature. The log–log plot of Fig. 15 illustrates the dynamical scaling theory of Hohenberg and Halperin (48) that predicts a critical slowing down of the fluctuating moments near T_f:

$$\tau_c = \tau_0 \left[\frac{T}{T - T_f} \right]^n. \qquad [4]$$

Attempts to describe meaningfully the temperature dependence of τ_c with Eq. [4] were unsuccessful. An exponent $n > 2$ was always required, implying that the critical slowing down of the spin fluctuations is very rapid. The inset of

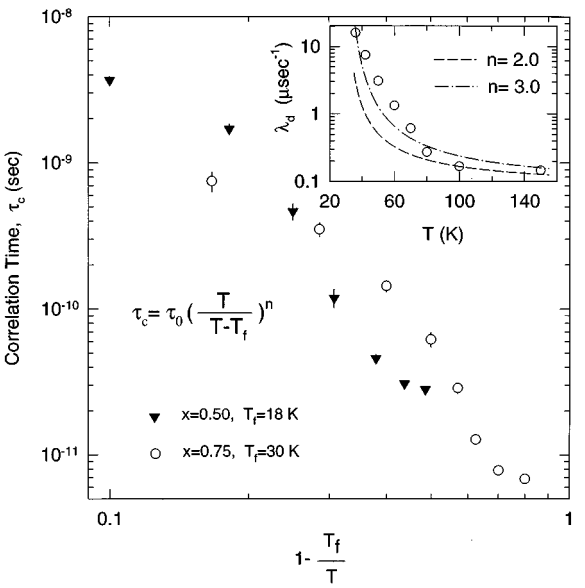

FIG. 15. Temperature dependence of the zero-field μ^+SR correlation time τ_c of the fluctuating moments in $La_2Co_{0.50}Cu_{0.50}O_{4.18}$ (▼) and $La_2Co_{0.75}Cu_{0.25}O_{4.16}$ (○). *Inset*: Power-law expressions for the $x = 0.75$ composition, with critical exponents $n = 2.0$ and 3.0.

Fig. 15 shows two power-law curves constrained to fit the high temperature points of $\lambda_d(\lambda_0 = 0.082\ \mu s^{-1})$ for $x = 0.75$. It shows clearly the complete failure of the $n = 2.0$ curve as the temperature approaches T_f, while the $n = 3.0$ one works somewhat better.

In the current discussion of the critical behavior of the correlation time, the possibility of a slight smearing of the critical temperature cannot be disregarded completely. It is an additional factor, which adds to the complexity of our data analysis. Even a small distribution of effective T_f values can have a fairly drastic effect on the analysis close to T_f. So, following the partial failure of the power-law behavior to describe the spin dynamics in $La_2Co_{0.75}Cu_{0.25}O_{4.16}$, especially close to the freezing temperature ($T \sim 1.2\,T_f$) where the correlation time strongly deviates from linearity, alternative modeling of the data was attempted with a standard Arrhenius law: $\tau_c = \tau_0 \exp(E_a/k_B T)$. This is much used in ordinary glasses to account for the increase in viscosity on approaching the glass transition temperature and is consistent with thermally activated processes involving constant (free) energy barriers. In order to account for the rapid change of the correlation time on approaching the freezing temperature, one has to involve a large activation energy (E_a). The correlation times on a logarithmic scale are plotted vs $1/T$ in Fig. 16. Linear behavior close to T_f is obtained, indicating the suitability of this model in determining the spin dynamics of the system. Nonlinear least squares fits between 36 and 80 K (or 22–29 K for $x = 0.50$) gave $E_a/k_B = 235(13)$ K ($\sim 8\,T_f$) and $\tau_0 = 1.2(4) \times 10^{-12}$ s. In the case of the $La_2Co_{0.5}Cu_{0.5}O_{4.18}$ sample, we find $E_a/k_B = 350(11)$ K ($\sim 19\,T_f$) and $\tau_0 = 2.0(1.1) \times 10^{-16}$. An Arrhenius law description of the correlation times derived by ZF-μSR is also valid in *Cu*Mn (5 atomic%) for which $E_a/k_B \sim 20\,T_f$ and $\tau_0 \sim 10^{-15}$ s, whereas in the amorphous Co aluminosilicate $(CoO)_{40}(Al_2O_3)_{10}(SiO_2)_{50}$ (Co 14.3 atomic %), $E_a/k_B \sim 13\,T_f$ and $\tau_0 \sim 10^{-12}$ s (25).

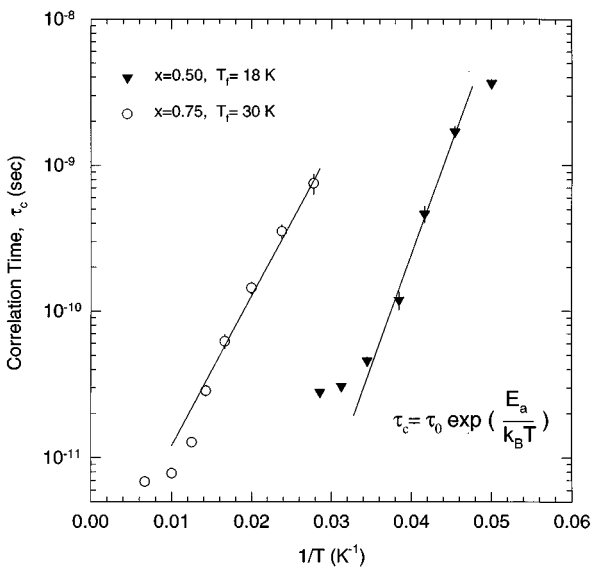

FIG. 16. Arrhenius plot of the zero-field μ^+SR correlation time τ_c vs inverse temperature in $La_2Co_xCu_{1-x}O_{4+\delta}$ ($x = 0.50$ (▼), 0.75 (○)).

This phenomenological approach in describing the spin freezing in spin glasses has been widely discussed (49) in terms of the Néel theory of supermagnetism. It is the short-range superexchange interactions that couple the local magnetic moments in the formation of a magnetic cluster. Thermal disorder opposes this tendency, whereas with decreasing temperature the regions of correlated spins becomes larger and the spin system is subdivided into independent magnetic clusters of different size. The freezing process can be understood as resulting from a distribution of temperatures at which the different magnetic clusters are no longer able to overcome an energy barrier and are therefore "blocked." If a cluster is blocked for a time greater than the time window of a typical measurement, it will appear "frozen" and will not be sensed by the measuring technique. The Néel theory of supermagnetism predicts that the relaxation time of a magnetic cluster follows an expression similar to the Arrhenius law quoted above.

The analytic expressions of describing the spin-freezing process above T_f are not completely undisputed. Although the Arrhenius expression describes τ_c well close to T_f, the activation energy obtained is unphysically large. In an effort to describe the strong temperature variation of the correlation time, the empirical Vogel–Fulcher law can be used: $\tau_c = \tau_0 \exp[E_a/k_B(T - T_0)]$, with T_0 a characteristic temperature introduced in an *ad hoc* fashion. The basic idea behind this law consists of building a magnetic superlattice of "blocked" moments when the freezing temperature is approached from above (21, 50). Its application to $La_2Co_{0.75}Cu_{0.25}O_{4.16}$ leads to a smaller value for the activation energy, $E_a/k_B = 21(4)$ K ($E_a/k_B = 18(2)$ K, $x = 0.50$) and a characteristic correlation time $\tau_0 = 2.4(1.3) \times 10^{-11}$ s ($\tau_0 = 2.0(9) \times 10^{-11}$ s, $x = 0.50$). Here we assumed $T_0 \approx T_f$. The Vogel–Fulcher (VF) law has described equally well the relaxation rate just above the freezing temperature $T_f = 44.0(5)$ K, of the insulating oxide spin glass $Fe_{1.75}Ti_{1.25}O_5$. The extracted activation energy $E_a/k_B = 20(5)$ K (21) agrees well with that found for $La_2Co_{0.5}Cu_{0.5}O_{4.18}$ and $La_2Co_{0.75}Cu_{0.25}O_{4.16}$.

On cooling below T_f, the dynamic depolarization rate $\lambda_d = 4\alpha_d^2/\nu$ decreases (Fig. 11), reflecting the rapid decrease in the dynamic field spread α_d. A contrasting behavior is shown above T_f, where the decrease in λ_d comes from the diverging character of the correlation time τ_c. On the other hand, the correlation time decreases slowly below T_f and is estimated to be of the order $\sim 10^{-10}$ s just below T_f, without much change from this value down to $T \sim 0.5\,T_f$ ($\tau_c = 1.4(4) \times 10^{-10}$ s for $x = 0.50$, $\tau_c = 1.9(7) \times 10^{-10}$ s for $x = 0.75$). Similar behavior was also found in the prototypical metallic spin glass *Cu*Mn (30) upon cooling below T_f.

All these properties governing the relaxation of the μ^+ spin polarization in $La_2Co_{0.5}Cu_{0.5}O_{4.18}$ and $La_2Co_{0.75}Cu_{0.25}O_{4.16}$, above and below the characteristic temperature T_f provide excellent evidence that the low-temperature magnetic state in the $La_2Co_xCu_{1-x}O_{4+\delta}$ layered oxides can be described as an Ising spin glass.

4. CONCLUSIONS

We have prepared a series of oxygen-rich phases with formal stoichiometry $La_2Co_xCu_{1-x}O_{4+\delta}$ that are isostructural with the $La_2CuO_{4+\delta}$ high-T_c superconductor. The concentration x vs transition temperature phase diagram (26) was determined by macroscopic ac and dc susceptibility measurements, whereas the local probe technique of muon-spin relaxation (μ^+SR) was employed to reveal the details of the microscopic physical mechanism governing the spin-freezing process in the materials. The mixed systems with Cu-rich concentrations exhibit antiferromagnetism (AF) in a similar fashion to the parent La_2CuO_4 phase. The transition temperature T_N from the paramagnetic (P) to the AF phase rapidly decreases with increasing Co concentration. The boundary between the P and AF phases appears to be smeared out when the Co concentration increases above 10%. For instance, a composition ($x = 0.25$) in the $0.2 < x < 0.5$ region exhibits dc susceptibility characteristic of static local magnetic moments of predominantly random order. In the intermediate and relatively high Co concentration region up to $x = 0.90$, we see a clear transition from the P to a spin glass (SG) state with very low freezing temperatures T_f. The freezing temperature is maximized for $La_2Co_{0.75}Cu_{0.25}O_{4.16}$. Finally, at the Co-rich end of the solid solutions, antiferromagnetic order is recovered again, but with a significantly suppressed Néel temperature compared to that of the stoichiometric La_2CoO_4 (14) compound.

The incorporation of a significant amount of excess oxygen ($0.06 \leq \delta \leq 0.20$) modifies the valence state of the transition metals. Divalent Co is more easily oxidized than divalent Cu ions. Such an effect gives rise to various electronic configurations (high- and/or low-spin states, see Table 4) so that some of the interactions of certain spin states with others favor ferromagnetic (F) and some antiferromagnetic exchange. These coexisting F and AF exchange interactions between nearest neighbors compete with each other, so that no spin configuration simultaneously minimizes its corresponding term in the spin Hamiltonian in order to establish an equilibrium magnetic ground state. With a distribution of F and AF bonds (coupling) at intermediate compositions, enough frustration of the original AF ground state is produced. As our neutron diffraction experiments have shown (12), the nonordered arrangement of Co in the Cu site for $La_2Co_xCu_{1-x}O_{4+\delta}$ solid solution leads to a site-random magnetic system where both ingredients of randomness and frustration are present. In conclusion, the suppression of the Néel state and the appearance of a spin glass ($0.5 \leq x \leq 0.9$) at very low temperatures in the $La_2Co_xCu_{1-x}O_{4+\delta}$ series can be attributed to increased degree of disorder among the (Co/Cu) sites and frustration of the nearest-neighbor AF bonds. Indeed, holes in the oxygen sublattice and/or randomization of possible low-spin Co^{II} states among the AF coupled Cu^{2+}, Co^{2+}, and Co^{3+} lattice sites may form ferromagnetic nearest-neighbor interactions that disrupt the otherwise AF, almost 2D network. It is proposed that ferromagnetic "clusters" are the building blocks out of which the spin glass state is established.

The spin dynamics probed by muon spin relaxation (μ^+SR) as the freezing temperature T_f is approached from above presents an example of a more universal behavior that has also been encountered in a variety of other spin glasses of diverse chemical composition. In agreement with a variety of literature results, the nonexponential ($G(t) = A_0 e^{-(\lambda_d t)^\beta}$) decay of the dynamic spin correlation function reflected in the zero-field μ^+SR and the rapid growth of the correlation times while approaching T_f from above are consistent with those of an Ising spin glass. Analysis of the dynamic μ^+ spin depolarization rate λ_d above T_f implies a critical slowing down of the spin fluctuations. When stretched exponential behavior sets in, as T is lowered toward T_f, the exponent β tends to a characteristic $\frac{1}{3}$ value. The spin glass freezing processes were discussed in terms of various phenomenological models. A simple Arrhenius law, encountered in the literature of common glasses, is more satisfactory in describing the dependence of the correlation time on T than a power law. Finally, the diminishing character of λ_d at $T < T_f$ is attributed to the reduction in the dynamic field distribution α_d and the simultaneous rapid increase of the static field spread α_s.

ACKNOWLEDGMENTS

Financial support from the TMR Programme of the European Commission (Research Network 'FULPROP' ERBFMRXCT970155) is acknowledged. K.P. thanks the Leverhulme Trust for a 1997–98 Research Fellowship. We also thank the Paul Scherrer Institute for the provision of muon beam time, A. Amato for help with the μ^+SR experiments, D. Herlach for technical support, and A. P. Ramirez for the SQUID susceptibility measurements.

REFERENCES

1. R. Schölhorn and P. Rudolf, *J. Chem. Soc. Chem. Commun.*, 1158 (1992).
2. B. O. Wells, R. J. Birgeneau, F. C. Chou, Y, Endoh, D. C. Johnston, M. A. Kastner, Y. S. Lee, G. Shirane, J. M. Tranquada, and K. Yamada, *Z. Phys. B* **100,** 535 (1996).
3. J. M. Tranquada, Y. Kong, J. E. Lorenzo, D. J. Buttrey, D. E. Rice, and V. Sachan, *Phys. Rev. B* **50,** 6340 (1994).
4. P. Ganguly, *in* "Advances in Solid State Chemistry" (C. N. Rao, Ed.); p. 135. Indian National Science Academy, New Delhi, 1986.

5. J. E. Schirber, B. Morosin, R. M. Merrill, P. F. Hlava, E. L. Venturini, J. F. Kwak, P. J. Nigrey, R. J. Baughman, and D. S. Ginley, *Physica C* **152,** 121 (1988).
6. J. W. Rogers Jr., N. D. Shinn, J. E. Schirber, E. L. Venturini, D. S. Ginley, and B. Morosin, *Phys. Rev. B* **38,** 5021 (1988).
7. J. Zhou, S. Sinha, and J. B. Goodenough, *Phys. Rev. B* **39,** 12331 (1989).
8. J. D. Jorgensen, B. Dabrowski, Shiyou Pei, D. R. Richards, and D. G. Hinks, *Phys. Rev. B* **40,** 2187 (1989); B. Dabrowski, J. D. Jorgensen, D. G. Hinks, S. Pei, D. R. Richards, H. B. Vanfleet, and D. L. Decker, *Physica C* **162–164,** 99 (1989).
9. J. D. Jorgensen, B. Dabrowski, S. Pei, D. H. Hink, L. Soderholm, B. Morosin, J. E. Schriber, E. L. Venturini, and D. S. Ginley, *Phys. Rev. B* **38,** 11337 (1994).
10. B. Morosin, G. H. Kwei, J. E. Schirber, J. A. Voigt, E. L. Venturini, and J. A. Goldstone, *Phys. Rev. B* **44,** 7673 (1991).
11. C. Rial, E. Morán, M. A. Alario-Franco, U. Amador, and N. H. Andersen, *Physica C* **254,** 233 (1995).
12. A. Lappas and K. Prassides, *J. Solid State Chem.* **108,** 59 (1994).
13. A. Lappas, D. Phil. thesis, University of Sussex, 1993.
14. K. Yamada, M. Matsuada, Y. Endoh, B. Keimer, R. J. Birgeneau, S. Onodera, J. Mizusaki, T. Matsuura, and G. Shirane, *Phys. Rev. B* **39,** 2336 (1989).
15. A. Schenck, *in* "Frontiers in Solid State Sciences," Vol. 2 (L. C. Gupta and M.S. Multani, Eds.). World Scientific, Singapore, 1993.
16. C.Dekker, A. F. M. Ares, H. W. Wijn, A. J. van Duyneveldt, and J. A. Mydosh, *Phys. Rev. Lett.* **61,** 1780 (1988).
17. E. J. Samuelsen, *Phys. Rev. Lett.* **31,** 936 (1973).
18. C. Dekker, A. F. M. Ares, and H. W. Wijn, *Phys. Rev. B* **38,** 8985 (1988); C. Dekker, A. F. M. Ares, and H. W. Wijn, *Phys. Rev. B* **38,** 11512 (1988).
19. K. Binder and A. P. Young, *Rev. Mod. Phys.* **58,** 801 (1986).
20. M. R. McHenry, B. G. Silbernagel, and J. H. Wernick, *Phys. Rev. B* **5,** 2958 (1978).
21. C. Boekema, V. A. M. Brabers, R. L. Lichti, A. B. Denison, D. W. Cooke, R. H. Heffner, R. L. Hutson, M. E. Schillaci, D. E. Maclaughlin, and S. A. Dodds, *Hyperfine Interact.* **31,** 369 (1986).
22. K. Emmerich, E. Lipplet, R. Neuhaus, H. Pnkvos, Ch. Schwink, F. N. Gygax, A. Hintermann, A. Schenck, W. Studer, and A. J. van der Wal, *Phys. Rev. B* **31,** 7226 (1985).
23. R. Kubo and T. Toyabe, *in* "Magnetic Resonance and Relaxation" (R. Blinc, Ed.). North-Holland, Amsterdam, 1967; R. Kubo, *Hyperfine Interact.* **8,** 731 (1981).
24. R. S. Hayano, Y. J. Uemura, J. Imazato, N. Nishida, T. Yamazaki, and R. Kubo, *Phys. Rev. B* **20,** 850 (1979).
25. Y. J. Uemura, *Hyperfine Interact.* **8,** 739 (1981).
26. A. Lappas, K. Prassides, A.Amato, R. Feyerherm, F. N. Gygax, and A.Schenck, *J. Magn. Magn. Mater.* **140–144,** 1291 (1995).
27. Y. J. Uemura, *Hyperfine Interact.* **17–19,** 447 (1984).
28. S. F. Edwards and P. W. Anderson, *J. Phys. F: Metal Phys.* **5,** 965 (1975).
29. Y. J. Uemura, Ph.D. thesis, University of Tokyo, 1982.
30. Y. J. Uemura, T. Yamazaki, D. R. Harshman, M. Senba, and E. J. Ansaldo, *Phys. Rev. B* **31,** 546 (1985).
31. Y. J. Uemura and T. Yamazaki, *Physica* **109–110B,** 1915 (1982).
32. A. T. Ogielski, *Phys. Rev. B* **32,** 7384 (1985).
33. R. V. Chamberlin, G. Mazurkevich, and R. Orbach, *Phys. Rev. Lett.* **52,** 867 (1984).
34. E. J. Vincent, J. Hammann, and M. Alba, *Solid State Commun.* **58,** 57 (1986).
35. E. Bartsch, A. Antonietti, W. Schupp, and H. Sillescu, *J. Chem. Phys.* **97,** 3950 (1992).
36. I. A. Campbell, A. Amato, F. N. Gygax, D. Herlach, A. Schenck, R. Cywinski, and S. H. Kilcoyne, *Phys. Rev. Lett.* **72,** 1291 (1994).
37. A. Keren, P. Mendels, and I. A. Campbell, *Phys. Rev. Lett.* **77,** 1386 (1996).
38. R. Cywinski and B. D. Rainford, *Hyperfine Interact.* **85,** 215 (1994).
39. J. R. Stewart, A. D. Hillier, S. H. Kilcoyne, R. Manuel, M. T. F. Telling, and R. Cywinski, *J. Magn. Magn. Mater.* **177,** 602 (1998).
40. I. A. Campbell, J.-M. Flesselles, R. Jullien, and R. Botet, *Phys. Rev. B* **37,** 3825 (1988).
41. B. J. Sternlieb, G. M. Luke, Y. J. Uemura, T. M. Riseman, J. H. Brewer, P. M. Gehring, K. Yamada, Y. Hidaka, T. Murakami, T. R. Thurston, and R. J. Birgeneau, *Phys. Rev. B.* **41,** 8866 (1990).
42. K. L. Ngai, *Comments Solid State Phys.* **9,** 127 (1979).
43. C. A. Angell, *in* "Relaxation in Complex Systems" (K. L. Ngai and G. B.Wright, Eds.). Office of Naval Research, Washinton, DC, 1984.
44. I. A. Campbell, and L. Bernardi, *Phys. Rev. B.* **52,** 9819 (1995).
45. N. Lemke and I. A. Campbell, *Physica A* **230,** 554 (1996).
46. B. Hitti, P. Birrer, K. Fisher, F. N. Gygax, E. Lippelt, H. Maletta, A. Schenck, and M. Weber, *Hyperfine Interact.* **63,** 287 (1990).
47. J. A. Mydosh, *in* "Heidelberg Colloquium on Glassy Dynamics" (J. L. van Hemmen and I. Morgenstern, Eds.). Springer-Verlag, Berlin, 1987.
48. P. C. Hohenberg and B. I. Halperin, *Rev. Mod. Phys.* **49,** 435 (1977).
49. P. J. Ford, *Contemp. Phys.* **23,** 141 (1982).
50. J. Souletie and J. L. Tholence, *Phys. Rev. B* **32,** 516 (1985).